Transportation Research Part D 139 (2025) 104541

Contents lists available at ScienceDirect

Transportation Research Part D

journal homepage: www.elsevier.com/locate/trd

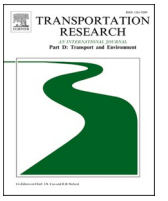

Modeling urban brake wear particle emissions: A ride-hailing case in Chengdu, China

Qiuzi Chen [a,b], An Wang [c], Shunyao Wang [d], Haobing Liu [e], Luyang Gong [f], Ran Tu [a,b,*]

[a] School of Transportation, Southeast University, Nanjing 211189, China
[b] Key Laboratory of Transport Industry of Comprehensive Transport Theory (Nanjing Modern Multimodal Transportation Laboratory), Ministry of Transport, PR China
[c] Department of Civil and Environmental Engineering, Hong Kong Polytechnic University, Hong Kong, China
[d] School of Environmental and Chemical Engineering, Shanghai University, Shanghai 200444, China
[e] The Key Laboratory of Road and Traffic Engineering, Ministry of Education, Tongji University, 4800 Caoan Road, Shanghai 201804, China
[f] China Academy of Transportation Science, Beijing, China

ARTICLE INFO

Keywords:
Brake wear particles
Non-exhaust emissions
Traffic emissions
Emission modeling
Spatiotemporal analysis

ABSTRACT

Brake wear particle (BWP) emissions, a major non-exhaust source of urban air pollution, will be regulated under Euro 7 standards. However, current knowledge on quantifying urban BWP emissions and their spatiotemporal variations is insufficient. This study incorporates an operating-mode-based modeling framework with large-scale ride-hailing trajectories and local survey data from Chengdu, China. The local PM_{10} emission factor was estimated to be 27 ± 4 mg/km/veh, higher than the literature due to frequent braking. By applying interpretable machine learning for trip-level analysis, strong correlations were identified between BWP emissions and driving characteristics like braking frequency, intensity, speed, and road grade, highlighting the need for reducing on-road braking through better driving and traffic management. Spatiotemporal analysis indicated emissions spike during congested hours, which are also highly correlated with sensitive spots like healthcare facilities. The results shed light on targeted strategies to mitigate the environmental and health impacts of BWP emissions.

1. Introduction

Non-exhaust emissions generated from brake, tire, road surface wear, and resuspended dust, account for up to 60 % by mass of total traffic-related particulate matter (PM) (Grange et al., 2021). This proportion is predicted to increase, accompanied by reduced regulated exhaust emissions (Sarica et al., 2024). One of the most important non-exhaust emissions sources is brake wear particle (BWP) emissions, contributing to the total non-exhaust PM_{10} emissions by 1.6 % to 55.3 % across various sampling locations (Harrison et al., 2012; Zhang et al., 2020). To this end, the Euro 7 standards have proposed setting an official regulation for PM from brakes of on-road vehicles, aiming to reduce 27 % of BWP emissions from cars and vans by 2035 (Ntziachristos et al., 2022).

BWP emissions are generated from the friction between vehicular brake pairs and influenced by factors such as initial speed,

* Corresponding author at: Modeling Urban Brake Wear Particle Emissions: A Ride-hailing Case in Chengdu, China.
E-mail addresses: qiuzi.chen@outlook.com (Q. Chen), an.wang@polyu.edu.hk (A. Wang), syw@shu.edu.cn (S. Wang), liuhaobing@tongji.edu.cn (H. Liu), 84142601@qq.com (L. Gong), turancoolgal@seu.edu.cn (R. Tu).

https://doi.org/10.1016/j.trd.2024.104541
Received 22 September 2024; Received in revised form 29 November 2024; Accepted 29 November 2024
Available online 19 December 2024

deceleration, brake pad materials, and vehicle load (Giechaskiel et al., 2024), for which it is difficult to capture the emission of every changing braking event. Based on single vehicle or brake pair wear tests, BWP emission models have been developed, such as the Motor Vehicle Emission Simulator (MOVES) (USEPA, 2020), the Computer Programme to Calculate Emissions from Road Transport (COPERT) (Ntziachristos and Boulter, 2023), and the EMission FACtors (EMFAC) (The California Air Resources Board, 2021). Given their application in regional emission quantification (Singh et al., 2020) and policy assessment (Chang et al., 2023), link-level BWP emissions have rarely been quantified in cities, where congestions occur frequently and the drive cycles are significantly distinguished from regulated models. Consequently, the relationship between BWP emissions and the features of aggregated vehicle operation (e.g., average speed, vehicle volume, and braking frequency) is challenging to assess precisely. Additionally, the spatial and temporal variations of BWP emissions on a finer scale are unclear. Current emission models also face limitations due to outdated data used in the current estimation models. These limitations hinder our understanding of BWP emissions and the development of effective mitigation measures.

To address these gaps, this study builds up a comprehensive modeling and analysis framework for network-wide on-road BWP emissions from light-duty vehicles (LDVs) in the urban area. This framework consists of an operating mode (OpMode) based BWP emission estimation model with the most recent measurement results and the multi-level trajectory aggregation technique. We apply this framework to a substantial ride-hailing trajectory dataset with local survey data in a central metropolitan area to investigate the influencing factors of BWP emissions and their spatiotemporal variations, based on which the implications of BWP mitigation strategies were discussed.

The rest of this paper is organized as follows. Section 2 briefly reviews the literature. Section 3 details the data used in this study and presents the modeling and analysis framework. The results are presented in Section 4, while Section 5 discusses the implications of mitigation policy and emission modeling. Section 6 summarizes the main findings and comments on the directions for future research.

2. Literature review

In this section, current BWP studies are reviewed from three aspects: influencing factors of BWP emissions, emission models for BWP, and the large-scale quantification of BWP emissions.

2.1. Influencing factors of BWP emissions

Research typically analyzes measurement results under various test conditions to summarize the influencing factors of BWP emissions from individual vehicles, including brake system attributes, vehicle weight, and braking behavior. Brake system attributes include brake pad materials (brake lining types) and brake types. Commonly used brake pad materials include semi-metallic (SM), low-metallic (LM), and non-asbestos organic (NAO), with distinct compositions and wear characteristics (Grigoratos and Martini, 2015). Generally, LM brake pads produce significantly higher emissions than SM and NAO brake pads (Woo et al., 2021). Morden LDVs typically use two brake system configurations: disc brakes and drum brakes (Grigoratos and Martini, 2015). Disc brakes are more common, but drum brakes, typically installed on rear wheels, have lower BWP PM emission factors but higher $PM_{2.5}$ content (Grigoratos et al., 2023).

Vehicle weight also influences BWP emissions. Increasing vehicle weight can significantly elevate emissions due to higher brake dissipation energy (Hagino et al., 2016). For instance, a 36 % increase in vehicle weight could result in a 23 % increase in PM_{10} emissions for metallic brake pads (Grigoratos et al., 2023). Consequently, heavy-duty vehicles usually exhibit higher on-road BWP emissions (Lee et al., 2023). The increased load on the battery also limits the emission reduction benefits of electric vehicles, depending upon the extent of regenerative braking (Beddows and Harrison, 2021).

Braking behavior parameters, including initial braking velocity, and braking deceleration, significantly impact BWP emissions. Generally, higher initial braking velocities and greater braking decelerations both lead to increased BWP emissions (Liu et al., 2022; Oroumiyeh and Zhu, 2021). Intense braking results in greater energy dissipation, further elevating BWP emissions (Wei et al., 2022).

Current research mainly focuses on individual vehicles or brake devices, providing a theoretical basis for emission models. However, there is a lack of exploration into the impact of macroscopic road characteristics, such as traffic volume, road grade, and average speed, which hinders the development of road-level mitigation strategies.

2.2. BWP emission models

Compared to exhaust emissions, the development of BWP emission models has relatively lagged on both model framework and measurement tests that were used to calibrate the model. Currently, only a few models provide the emission factors (EFs) or emission rates (ERs) for BWP, including COPERT, EMFAC, and MOVES series. The COPERT model, developed by the European Environment Agency (EEA), and the EMFAC model, developed by the California Air Resources Board (CARB), calculate BWP emissions based on vehicle type and average speed (Ntziachristos and Boulter, 2023). Compared to COPERT and EMFAC, MOVES4, the most updated MOVES version, offers instantaneous input options and can estimate EFs based on vehicle driving characteristics. Different from the other two models, MOVES4 uses second-by-second speed and acceleration to determine instantaneous OpModes, which correlates to the power need and the value of BWP ER (USEPA, 2020).

These models have been utilized worldwide. However, the latest measurement data used in COPERT and MOVES4 dates back to 2001, making it outdated for the current vehicle specifications (Garg et al., 2000; Sanders et al., 2003). Although EMFAC updated its measurements in 2021, the testing was conducted within the context of California, including test vehicles and the driving cycle. Its

application to regions outside of California requires further verification.

2.3. Spatiotemporal distribution of BWP emissions

The quantification of the spatiotemporal distribution of BWP emissions is crucial for regional pollution analysis and emission mitigation policies. The source apportionment analysis based on roadside sampling and air contaminant tests has been widely used in the past (Jeong et al., 2019; Matthaios et al., 2022). However, BWP tracers (e.g., iron, copper, and titanium) in the atmospheric environment can also be associated with other pollution sources such as industry and construction, introducing a wide variation to the result of source apportionment across regions. In addition, this method requires a substantial number and duration of samples, making it challenging to achieve large-scale representative quantification (Piscitello et al., 2021).

Another approach applies the aforementioned emission models with vehicle information and road traffic data. For example, using EFs and road traffic volume data, a study found that the arterial roads are the primary emission source in Delhi, India, while the national highway has the highest EF (Singh et al., 2020). Considering vehicle driving distances, rural roads in India significantly contribute to non-exhaust emissions (Tomar et al., 2022).

While the application of EFs and emission models supports city-scale, detailed analysis, current research often uses a uniform EF from existing models, overlooking differences in EFs caused by regional traffic variation, which is differentiated by the drive cycle, vehicle fleet distribution, and time-varying traffic conditions.

3. Methodologies

In this study, a systematic methodology consisting of data processing, model development, and multi-level aggregation analysis is proposed and presented in Fig. 1. Three categories of data are required, including the vehicle activity data extracted from vehicle trajectory, vehicle curb weight, brake types, and the market share information of brake pad materials based on local surveys. These data serve as the inputs of the OpMode-based model to estimate the vehicle-level BWP emissions. Based on the above data and models, a spatiotemporal analysis is applied to identify traffic and driving factors that affect vehicle BWP and mitigation efforts can be derived herein.

3.1. Vehicle activity

3.1.1. Trajectory data processing

The vehicle activity data describe the typical characteristics of driving and braking behaviors (idling, coasting, acceleration, braking, etc.) for drivers in a specific region. In this study, vehicle activity was extracted from ride-hailing GPS data due to their sufficient sample size and extensive road network coverage (Wu et al., 2023). A 30-day ride-hailing trajectory dataset from November 1 to November 30, 2016, in Chengdu, China, was adopted to obtain the required driving activity data. The dataset was provided by DiDi (https://web.didiglobal.com/), a company that offers app-based ride-hailing services across the country, which are performed by registered taxis and regular passenger cars (Sun et al., 2018). As shown in Fig. 2, the dataset covers a 70 km^2 area in downtown metropolitan Chengdu. The location coordinates, timestamps, and vehicle IDs of more than 200,000 ride-hailing orders per day were recorded with a frequency of 2 to 4 s, consisting of 1.097 billion data records in total.

The trajectory data were processed by the following steps, including encoding, segmentation, map-matching, densification,

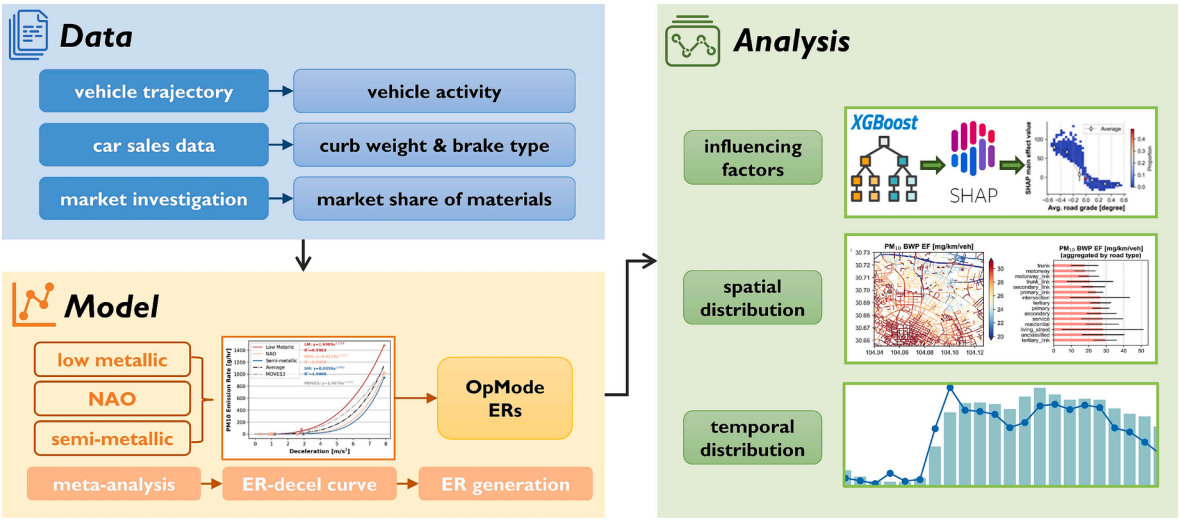

Fig. 1. Flowchart of the methodology in this study.

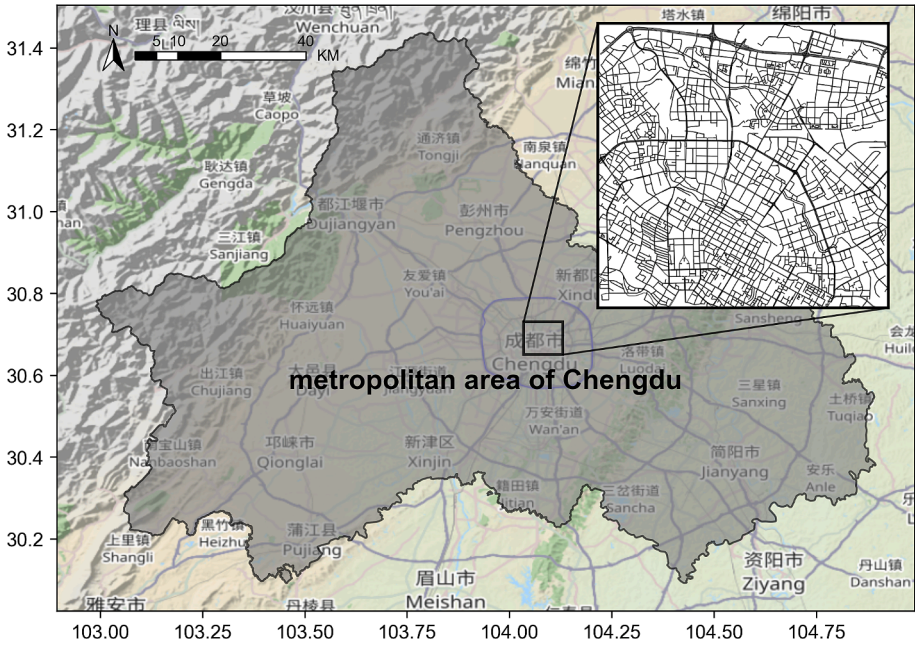

Fig. 2. Illustration of the study area and the road network of the metropolitan area.

calculation, smoothing, and filtering. In the map-matching procedure, trajectory points were aligned to the road network by PyTrack, an open-source map-matching Python toolbox (Tortora et al., 2022). Kinematic parameters, including speed, acceleration, and vehicle-specific power (VSP, in Eq.S1), were then calculated with the second-by-second driving record. The road grade, defined as the angle of the elevation to the horizontal distance between two trajectory points in this study, was extracted from the 12.5-meter Digital Elevation Model proposed by Alaska Satellite Facility (Alaska Satellite Facility, 2015). Details of processing steps are described in S1 of the Supporting Information. In total, over 2.96 billion processed and map-matched trajectory samples from an average of 39,189 vehicles per day were obtained from the raw dataset. Note that more aggressive acceleration and braking behaviors may be observed in the dataset due to more experienced drivers of ride-hailing vehicles. Nevertheless, the speed interpolation was performed to fill the missing time points, which smooths potential aggression.

3.1.2. OpMode distribution and braking profile

Two types of vehicle activity data were obtained from the processed trajectory data, including the OpMode distribution and the braking profile.

OpModes are defined to represent driving conditions and each of them is associated with an ER for each vehicle type with a specific fuel type. We assigned trajectory points to each OpMode according to the definition in MOVES4, the most widely used OpMode-based model. A total of 23 OpModes (see S2) were defined for light-duty running emissions with three types of operations: braking, idle, and cruise-acceleration, which were further separated into different speed and acceleration bins.

The braking profile contains the braking frequency (#/km), braking fraction, and the distribution of braking deceleration (m/s^2) of the studied fleet. The braking frequency refers to the number of consecutive braking events within a unit distance. For second-by-second data, the braking fraction is equivalent to the ratio of braking time during driving. These data describe how often and how hard vehicles brake, and are used for adjusting the OpMode ERs. To distinguish braking and coasting in the deceleration phase, a coastdown curve generated from the Physical Emission Rate Estimator was used (USEPA, 2020). All trajectory points with deceleration below the coastdown curve were assumed as braking and otherwise low throttle deceleration.

3.2. Brake and vehicle specifications based on local survey data

Using online data mining techniques, we obtained the local distribution of vehicle curb weights, brake types, and the market share of various brake pad materials. This comprehensive survey ensures our emission estimates are grounded in the local context.

The curb weight and brake type used for the ride-hailing fleet were obtained from Auto Home (https://www.16888.com/), a website that provides monthly car sales data in China. We collected vehicle model sales and configuration parameters from January 2015 to November 2016 to represent the fleet characteristics in Chengdu as of November 2016, Four classes were considered: small car (A0), compact car (A), mid-size car (B), and large car (C) (China Automotive Technology and Research Center, 2022). The detailed definitions of these classes are listed in S3. Only internal combustion engine vehicles were considered due to the low market share (less than 2 %) of electric vehicles at that time (Du and Ouyang, 2017). Sales data, curb weight, and front and rear brake type of 231 models in total were extracted.

Due to the lack of detailed investigation into the Chinese brake pad market, we conducted a survey using JD Mall (https://www.jd.com), one of China's largest e-commerce platforms, offering over eight thousand brake pad products from 17 brands. We used the keyword "car brake pads" and selected parameters, including brand, material, and axle (front or rear), to obtain product information. The number of comments was extracted to determine product popularity, which is highly correlated with sales (Ren et al., 2018).

The sales-weighted average curb weight of internal combustion engine LDVs is 1,350.98 kg, which is close to that in MOVES4 (1,497 kg) when considering the load of driver and passengers. Fig. 3 (a) shows the brake type ratio for both front and rear brakes. All LDVs use disc brakes on the front wheels, while 22.28 % use drum brakes on the rear wheels. Some studies indicated that the BWP emissions from drum brakes of the same vehicle type are about 12.05 % to 46.67 % of those from disc brakes (Garg et al., 2000; Grigoratos et al., 2023; Storch et al., 2023). These results were used to adjust the estimated ERs in the model (Section 3.3). Fig. 3 (b) shows that NAO brake pads dominate the Chinese market, with a market share of over 79 % for both front and rear brakes. SM brake pads have the lowest market share at less than 3 %, while the LM brake pads have a similar market share for front and rear brakes at about 17 %. Note that we included ceramic brake pads in the NAO category due to their comparable BWP emissions (Zhang et al., 2024a).

3.3. BWP emission calculation

An OpMode-based BWP emission modeling framework was adopted in this study, which calculates on-road BWP emissions by associating OpModes with ERs (g/hr/veh) to represent the "fleet average" emissions for specific driving behaviors. The modeling framework was derived from that in MOVES4, which consists of two main procedures: fitting the ER-deceleration curve and assigning ERs to OpModes. As shown in Fig. 4, several modifications were made to the modeling framework in this study and will be illustrated in Sections 3.3.1 and 3.3.2.

3.3.1. Fitting the ER-deceleration curves

The ER-deceleration curves were fitted to estimate individual and instantaneous ERs at different deceleration rates to illustrate the relationship between the average BWP ER and the average deceleration of braking of driving cycles. They were derived through a *meta*-analysis of published articles that include measurements from brake dynamometer tests over the past 20 years. Given the impact of brake pad materials on the BWP emissions, ER-deceleration curves were fitted for three materials (NAO, LM, and SM), respectively. S4 details the review process and summarizes the data from the *meta*-analysis.

Before fitting the curves, we first converted each measurement result to an EF of a single front brake, which was then converted to an ER (mg/hr/brake) based on the test cycle parameters. A detail of the EF-ER transformation is provided in S4. We then obtained the vehicle-level ER-deceleration curves through additional mixing and adjusting procedures that follow the assumptions based on the local survey data:

a. 2/3 of the braking power (and thus emissions) is in front brakes and 1/3 in rear brakes, so the ER of rear brakes is assumed to be 50 % of the ER of front brakes (Grigoratos et al., 2023).
b. The market share of NAO, LM, and SM is 79.74 %, 17.75 %, and 2.51 % for front brakes; 81.87 %, 17.55 %, and 0.58 % for rear brakes based on the local market survey.
c. All front wheels use disc brakes, 77.72 % of rear wheels use disc brakes, and 22.28 % of rear wheels use drum brakes. It is also assumed that the PM_{10} BWP emissions of each rear drum brake are 30 % of the emissions of the rear disc brake.

The mixing and adjusting procedures were performed by Eq. (1) to Eq. (4) where d denotes the deceleration (m/s^2). $ER^{disc}_{front}(d)$,

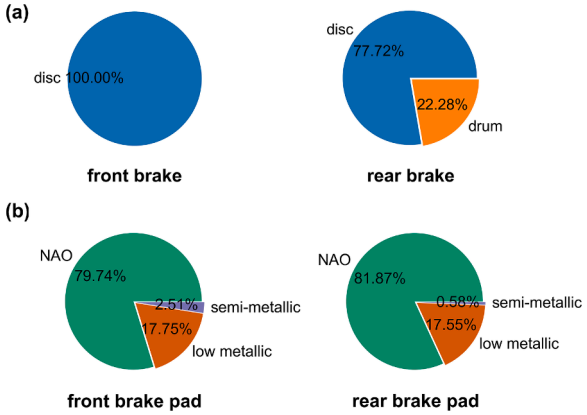

Fig. 3. Local survey results of (a) front and rear brake type ratio of internal combustion engine LDVs in the Chinese market from January 2015 to November 2016, and (b) market share of brake pad materials for front and rear brakes from comments data in JD Mall, representing the market preference in China.

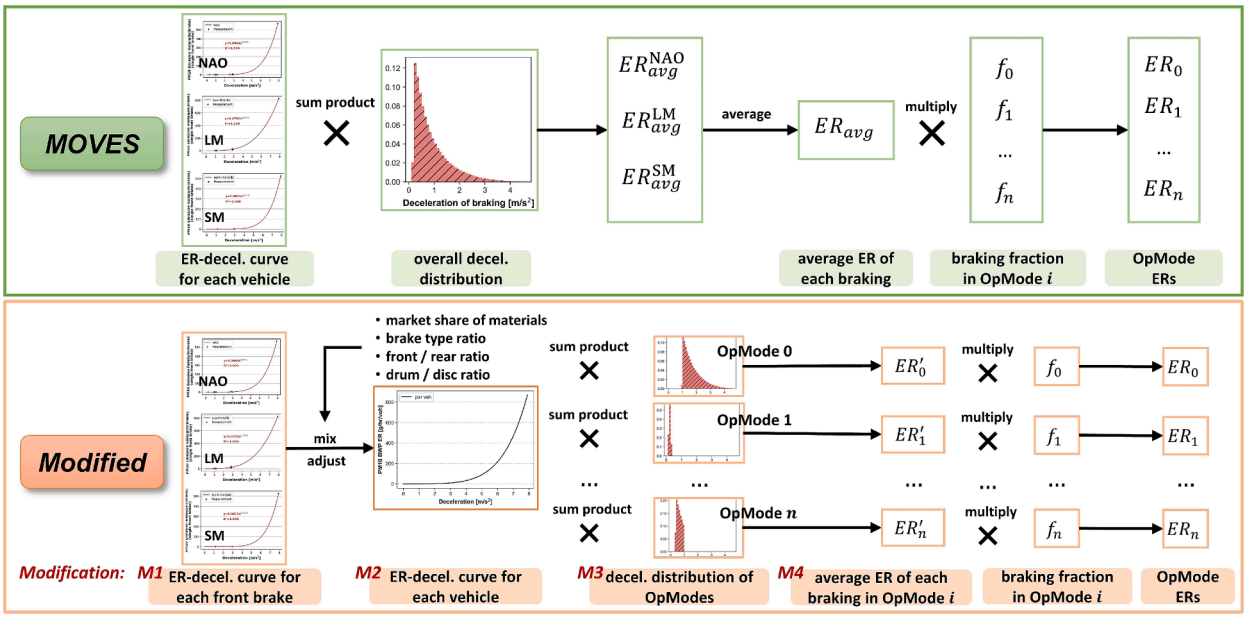

Fig. 4. Graphical illustration of OpMode ERs calculation in MOVES (top) and this study (bottom). Four modifications were made compared to MOVES: *M1*. ER-deceleration curves were updated for each front brake based on the most recent measurements; *M2*. An ER-deceleration curve for each vehicle was derived by mixing and adjusting according to local survey data; *M3*. Unique braking deceleration distributions for each OpMode were considered, rather than using an overall distribution. *M4*. The average ER of each braking was derived for each OpMode instead of using an average across all trajectories.

$ER^{disc}_{rear}(d)$, $ER^{drum}_{rear}(d)$, and $ER_{veh}(d)$ denote the ER-deceleration curve (function) of single front disc brake, rear disc brake, rear drum brake and the vehicle-level ER, respectively. Eq. (1) and Eq. (2) are consistent with assumptions a and b while Eq. (3) and Eq. (4) are consistent with assumption c.

In Eq. (1), the ER-deceleration curves from a single front brake of three materials were mixed to an average curve for a single front disc brake according to the market share in assumptions *b*. The same procedure was performed for the rear disc brake with an assumed rear/front BWP emission ratio of 50 % in assumptions *a* for adjustment. The assumed drum/disc BWP emission ratio and brake type ratio in assumption *c* was used for generating the curve for a single rear drum brake in Eq. (3) and calculating the curve for a single vehicle in assumption Eq. (4). An uncertainty analysis of the calculation and assumptions, provided in S11, estimates the potential bias for OpMode ERs ranges from −12 % to + 17 %, while the bias for the average EF ranges from −3.3 to + 4.1 mg/km/veh.

$$ER^{disc}_{front}(d) = 79.74\% \cdot ER^{front}_{NAO}(d) + 17.75\% \cdot ER^{front}_{LM}(d) + 2.51\% \cdot ER^{front}_{SM}(d) \quad (1)$$

$$ER^{disc}_{rear}(d) = 50\% \cdot \left(81.87\% \cdot ER^{front}_{NAO}(d) + 17.55\% \cdot ER^{front}_{LM}(d) + 0.58\% \cdot ER^{front}_{SM}(d)\right) \quad (2)$$

$$ER^{drum}_{rear}(d) = 30\% \cdot ER^{disc}_{rear}(d) \quad (3)$$

$$ER_{veh}(d) = 2 \cdot ER^{disc}_{front} + 2 \cdot \left(77.72\% \cdot ER^{disc}_{rear} + 22.28\% \cdot ER^{drum}_{rear}\right) \quad (4)$$

The vehicle-level ER-deceleration curve was fitted with the above assumptions and shown in S4. Note that the scope of analysis in this study included only PM_{10} due to insufficient evidence to estimate the EF of $PM_{2.5}$, with its proportions relative to PM_{10} ranging from 30 % to 80 % (Garg et al., 2000; Iijima et al., 2008; Storch et al., 2023; Woo et al., 2021).

3.3.2. *OpMode ERs assignment*

In this study, we consider the non-uniform braking deceleration distribution in different OpModes, distinguishing from MOVES4 which assigns a certain proportion of braking in each OpMode and an average ER of all braking events. This modification enables a more accurate ER estimation according to different levels of deceleration as formulated in Eq. (5), where ER_i is the ER (g/hr/veh) of OpMode *i*. For OpMode *i*, f_i represents the braking fraction and $p_{i,d}$ represents the proportion of braking records with deceleration of $d \in D$ among all braking records in this OpMode. The corresponding ER value of deceleration $d \in D$ on the ER-deceleration curve is denoted as $ER_{veh}(d)$.

$$ER_i = f_i \times \sum\nolimits_{d \in D} p_{i,d} \cdot ER_{veh}(d),\ \forall i \in OpModes \quad (5)$$

After assigning ERs to each OpMode, the total BWP emissions *TE* (g) at different aggregation scales (e.g., links, periods, and trips) can be calculated by Eq. (6) where t_i (hour) is the source hour of OpMode *i*. The corresponding EF (mg/km/veh) is then given by Eq. (7) where *D* is the total mileage of vehicles (km) within a certain spatiotemporal frame.

$$TE = \sum_{i \in OpModes} t_i \cdot ER_i \tag{6}$$

$$EF = \frac{TE}{D} \times 1000 \tag{7}$$

3.4. Trip-based analysis and explainable machine learning

To explore the relationship between driving behavior and BWP emissions, a trip-based analysis based on explainable machine learning was conducted. The processed data was divided into 500-meter trip segments, covering 2 to 3 urban blocks, to ensure sufficient variation and braking events. Trip-level features, as listed in Table 1, were then calculated. Due to computational constraints, we selected trajectory data from November 20 for analysis, as it had a near-average data volume and braking fraction. This resulted in 1.1 million trip segments being extracted from the trajectory data.

Trip segment data containing any braking event were used to train and test the XGBoost regression model, with the trip-based PM_{10} BWP EF as the dependent variable. The performance of the XGBoost model has been demonstrated in various machine learning problems (Chen and Guestrin, 2016). Tree-based models, including the XGBoost, can be more accurate than deep learning models on tabular-style datasets, and more interpretable than linear models due to model-mismatch effects (Lundberg et al., 2020).

Eighty percent of all samples were randomly selected for training and validation, while the remaining twenty percent were used for testing. A grid search method with the 10-fold cross-validation was employed to tune the hyper-parameters of XGBoost with R^2 as the evaluation metric. Both R^2 and root-mean-square-error (RMSE) were used to evaluate the model performance. They were calculated by Eq. (8) and Eq. (9) where y_i is the true value, $\hat{y}_i$ is the corresponding predicted value of the *i*-th trip segment, and $\bar{y}$ is the mean EF of all *N* samples. The closer the R^2 is to 1 and the RMSE is to 0, the better the model's prediction performance.

$$R^2(y, \hat{y}) = 1 - \frac{\sum_{i=1}^{N} (y_i - \hat{y}_i)^2}{\sum_{i=1}^{N} (y_i - \bar{y})^2} \tag{8}$$

$$RMSE = \sqrt{\frac{\sum_{i=1}^{N-1} (y_i - \hat{y}_i)^2}{N}} \tag{9}$$

The well-trained model approximates the relationship between features and EFs, and its explanation involves understanding how the model uses input features to make predictions. To better understand the impact of driving, braking, and road characteristics on PM_{10} BWP EFs, the TreeExplainer in the SHAP (SHapley Additive exPlanations) framework was adopted (Lundberg et al., 2020). Based on the cooperative game theory, this framework computed SHAP values for features in all samples representing their contributions to the trip EF. Due to computational constraints, 100,000 samples were randomly selected to generate SHAP values. The summary plot and dependence plot were employed to reveal the global importance of each feature, and the local feature dependence with individual variability. It should be noted that although this method is widely used in many studies on nonlinear relationships between variables, its results should be considered as inferences rather than verified conclusions, which need sufficient measurements and robustness validation.

Table 1
Features and variables for training the XGBoost regression model.

Category	Features	Description	Unit
Dependent variable	PM_{10} BWP EF	The PM_{10} BWP EF of a trip.	mg/km/veh
Driving behaviors	Avg. speed	The average speed in a trip.	km/h
	Speed std.	The standard deviation of speed.	km/h
	Avg. acceleration	The average acceleration in a trip.	m/s^2
	Acceleration std.	The standard deviation of acceleration.	m/s^2
	Avg. VSP	The average VSP in a trip.	kW/t
	VSP std.	The standard deviation of VSP.	kW/t
Braking behaviors	Avg. decel. of braking	The average deceleration of braking.	m/s^2
	Avg. duration of braking	The average duration of braking.	s
	Braking frequency	Number of braking events per kilometer.	#/km
	Avg. initial speed	The average initial speed of braking events.	km/h
	Idling fraction	Fraction of idling time in a trip.	–
Road characteristics	Avg. road grade	The average road grade of a trip.	degree
	Road grade std.	The standard deviation of road grade.	degree

3.5. Multi-level temporal and spatial aggregation analysis

In this study, trajectory data were aggregated temporally by each day of the week and each hour of the day, and spatially by street level and road types. At each aggregation level, statistics for driving, braking, and road characteristics, and the BWP emissions were calculated. The map-matching process assigned each trajectory sample to road segments based on the coordinates. In this study, 14 road types listed in S6 were identified through map-matching and road geometry acquisition from OpenStreetMap (https://www.openstreetmap.org/). A road map indicating the road type classification is shown in Figure S6-1. Urban intersections were classified as nodes in the road network with two or more edges due to unique trajectory features at intersections. For each intersection, trajectories within a 20-meter radius were aggregated to represent its characteristics. Total BWP emissions of each road section were then mapped with the Point-of-Interest (POI) extracted from OpenStreetMap to reveal the geographical correlation between BWP hotspots and specific land use types.

4. Results

4.1. Network-wide PM_{10} BWP EF

Using the ER-deceleration curve and braking profile, we assigned ERs to each OpMode (see S7) to estimate the network-wide PM_{10} BWP EF in the study area. The trajectory-volume-weighted average PM_{10} BWP EF of ride-hailing vehicles on all road segments, calculated by Eq. (7), reaches 27 ± 4 mg/km/veh. While the average BWP emissions per braking in this study align with some laboratory measurements at 1.7 mg (Garg et al., 2000; Sanders et al., 2003), the estimated EF significantly exceeds existing measurements in brake dynamometer studies (2.9 to 8.1 mg/km/veh) and emission inventories (7 to 18.5 mg/km/veh).

Notably, in our research scenario, the average initial vehicle speed of braking (28.74 km/h) and average deceleration (0.83 m/s^2) are comparable to laboratory test cycle settings (see Table S7–S3). The elevated EF likely results from the high braking frequency of the ride-hailing vehicles in the metropolitan area studied, where 85 % of the roads in the study area are urban unrestricted roads with disruptions, such as intersections and pedestrian crossings. Consequently, the proportion of braking behaviors on unrestricted roads is higher than on restricted roads such as motorways and expressways (Zhai et al., 2019). A source apportionment study also shows that PM_{10} BWP EF in urban streets could be much higher than on freeways (Bukowiecki et al., 2010). Additionally, taxi or ride-hailing drivers tend to accelerate and decelerate more frequently to gain speed advantages in congestion, resulting in higher deceleration/braking fractions (30 % higher on average) (Zhai et al., 2019). We also found that the braking frequency in this study is much higher than common test cycles, averaging 15.10 per km, compared to regulatory drive cycles (e.g., 1.47 for 3 h-LACT, 1.56 for WLTP-Brake, 1.82 for NEDC, 4.08 for WLTC (class 3), and 5.51 for FTP-75) (Chen and Tu, 2024). The evidence explains that the estimated EF is higher than the literature, and provides a valuable reference for quantifying BWP emissions in urban areas. Nevertheless, more empirical verification is required in future experiments.

4.2. Impact of trip-based features on BWP emissions

Figure S5 demonstrates the prediction performance of the XGBoost regression model in which the estimated EFs matched well with the true values with an R^2 of 0.95 and an RMSE of 6.82 mg/km/veh. The SHAP summary plots in Fig. 5 indicate that the average road grade is the most important feature influencing the trip-based EF. Driving characteristics including the braking frequency, the average

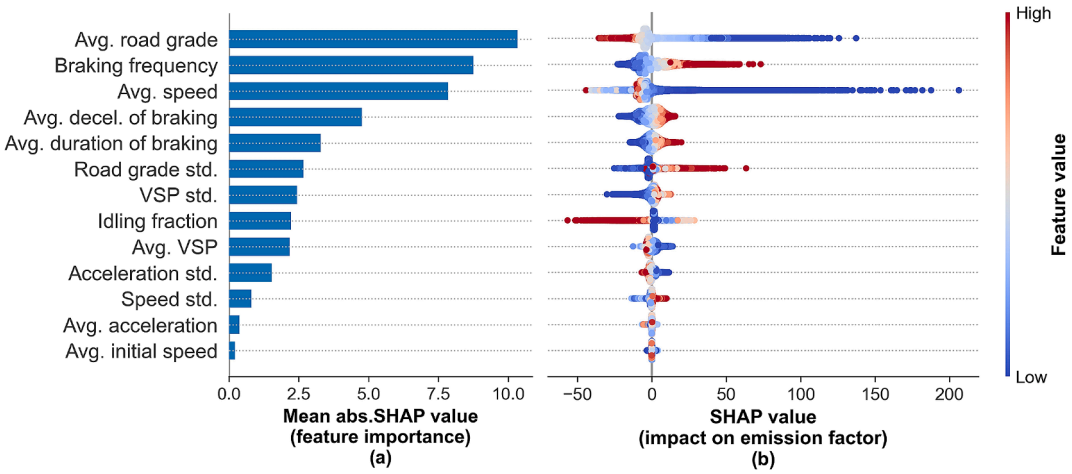

Fig. 5. SHAP summary plot of (a) the global feature importance; and (b) distribution of SHAP values along with feature values. Each dot is colored by the value of that feature from low (blue) to high (red). The closer to the right on the horizontal axis, the greater the SHAP value of this feature value to EF.

speed, the average deceleration of braking, and the fraction of braking also have a high impact on BWP emissions. Fig. 5 (b) illustrates the individual impact of each feature on the trip-based EF for all samples. Each dot is colored by the feature value, ranging from low (blue) to high (red), with dots positioned further to the right on the horizontal axis indicating a higher contribution for that feature to EF. For example, the higher the braking frequency, the larger the SHAP value, indicating a positive effect on EF, whereas a lower braking frequency corresponds to a smaller EF.

The SHAP dependence plots of the top 6 important features are shown in Fig. 6. The most influential factor is road grade, whose impact can be elaborated from two aspects. First, a negative average road grade tends to increase the EF (Fig. 6 (a)) due to intense braking behavior when driving downhill. This is opposite to exhaust emissions, which rise when driving uphill due to high engine load (Gallus et al., 2017; Liu et al., 2019a). Second, variations in road grade lead to higher BWP emissions (Fig. 6 (b)) because they indicate more downhill grades and potential braking events.

The influence of braking parameters is shown in Fig. 6 (c), (d) and (e). Frequent braking with aggressive deceleration and long duration leads to high trip BWP emissions. Although frequent braking is usually found to be short and gentle (Figure S9-1), it still generates high BWP emissions, implying more significant effects of braking frequency than individual braking intensity and duration. This finding extends the result of previous research emphasizing the impact of braking intensity (Liu et al., 2022; Oroumiyeh and Zhu, 2021; Wei et al., 2022; Woo et al., 2021).

The average speed is strongly correlated with BWP emissions. Fig. 6 (f) illustrates that when the average speed is lower than 20 km/h, there is a positive marginal effect on the EF. As speed increases, this effect gradually weakens, stabilizes, and eventually leads to a slight reduction in EF. Although some dynamometer studies have found that higher initial braking speed, which is proportional to the average speed (Figure S9-2 (a)), will increase BWP emissions per braking (Kim et al., 2020; Woo et al., 2021), the impact of speed may be different when considering trip-level emissions. By examining the distribution of OpModes, we found that at high speed, the proportion of coast and cruise/acceleration OpModes increases, while the proportion of the braking OpMode decreases (Figure S9-3). Another evidence lies in the relationship between speed and braking frequency (Figure S9-2 (b)). The higher the driving speed, the lower the braking frequency. In other words, driving at a low speed on urban roads generally involves frequent braking whose positive effect on BWP EF was unveiled by the SHAP value. However, despite the reduced BWP emissions per braking event at low speeds, the cumulative effect of frequent braking still results in higher overall BWP emissions.

4.3. Spatial BWP emission variations

After the spatial aggregation, the driving, braking parameters, and BWP EFs were assigned to the 2,409 road segments and 2,836 intersections in the study area. The average length of street segments is 679.2 m. Fig. 7 (a) displays the PM_{10} EF of each street and road type. The blue color of the 3rd ring road, the most important motorway in the Chengdu urban area, indicates its low EF, which contrasts with the high EFs of the intersecting urban streets. The results of road type aggregation also show that the average EFs of motorways and trunks are lower than 18 mg/km/veh, while the EFs of unrestricted roads are generally higher, followed by intersections. This difference is amplified by the accumulation of trajectory volume. As shown in Fig. 7 (b) and (c), the daily PM_{10} BWP emissions are mostly contributed by arterial roads with dense traffic and high EF, including primaries, secondaries, and tertiaries.

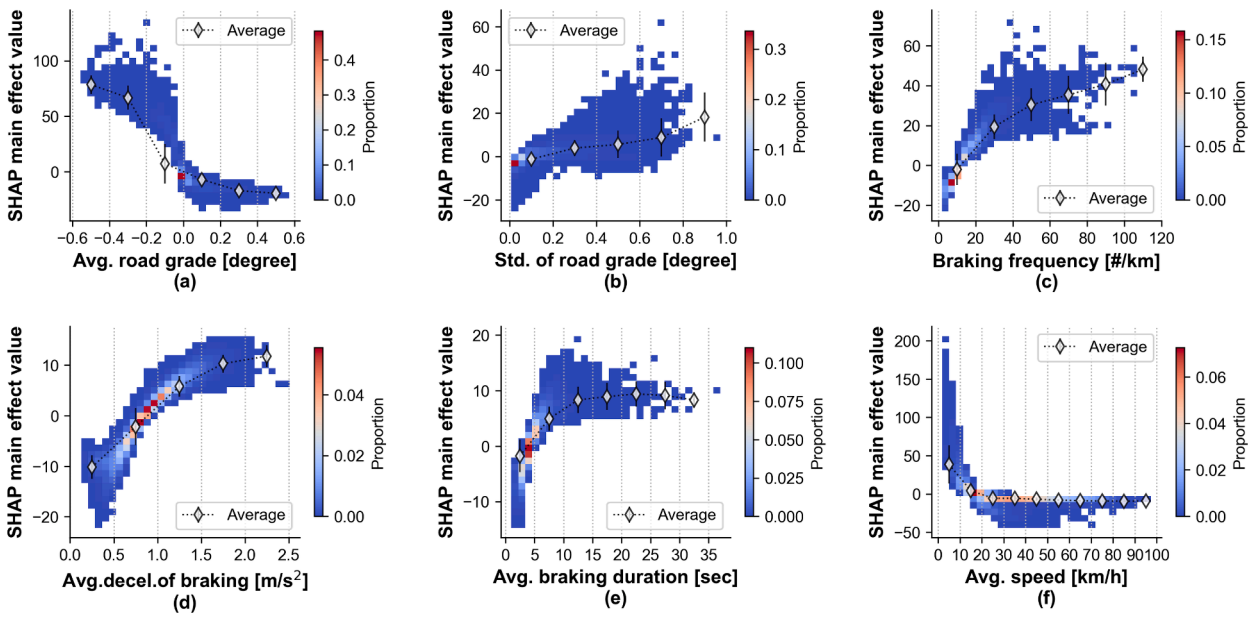

Fig. 6. SHAP dependence plots of the top-6 important features: (a) the average road grade; (b) the standard deviation of road grade; (c) braking frequency; (d) the average deceleration of braking; (e) the average braking duration; and (f) the average speed.

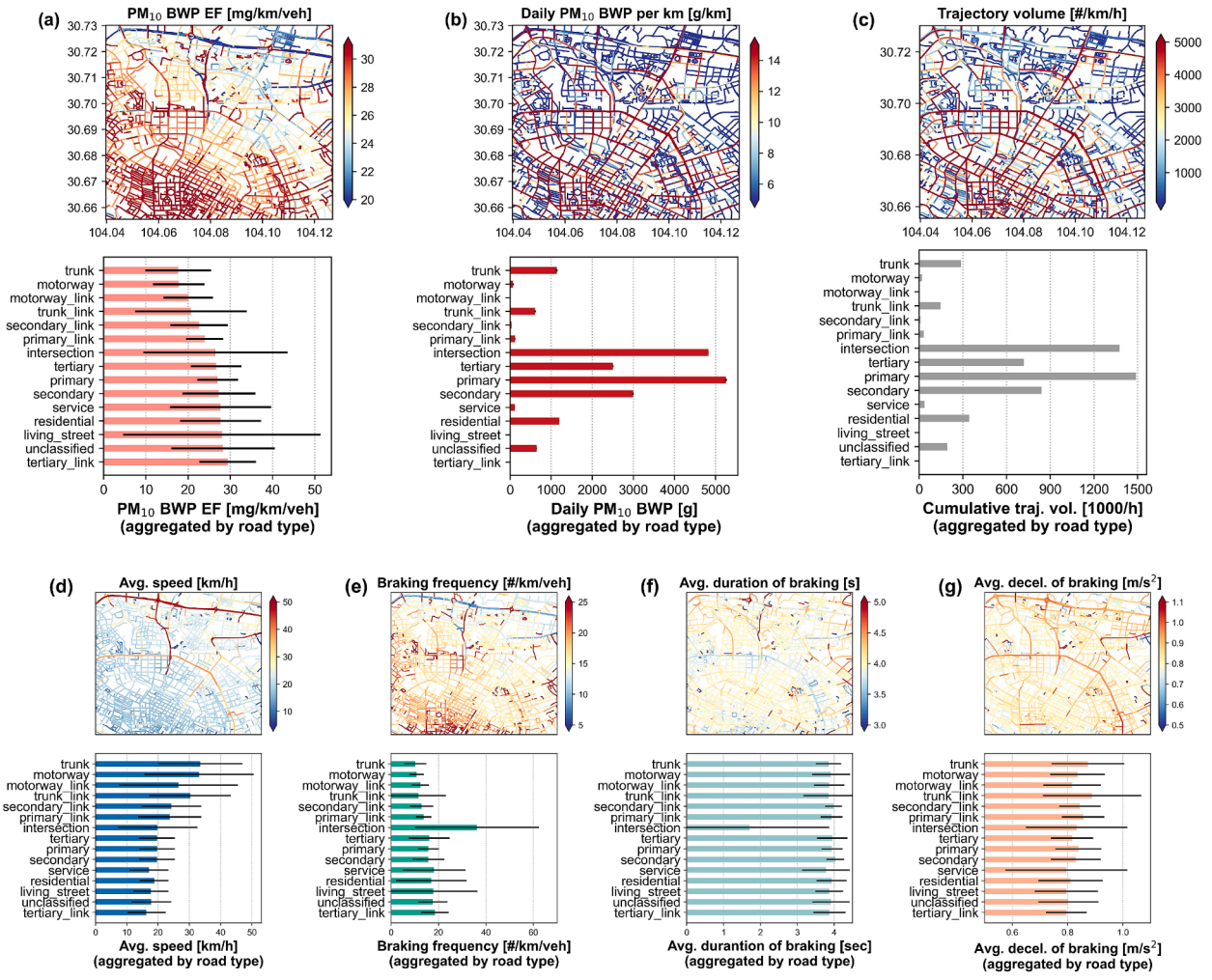

Fig. 7. The spatial distributions and road type aggregation results of (a) PM_{10} BWP EF; (b) daily PM_{10} BWP emissions; (c) trajectory volume; (d) the average speed; (e) braking frequency; (f) the average duration of braking; and (g) the average deceleration of braking in the study area. Road types are sorted by the average PM_{10} BWP EF.

Another significant contributor is intersections, which generated 32.9 % of the total. In contrast, BWP emissions are relatively low in residential streets due to low traffic volume. Note that this total BWP emissions only includes ride-hailing vehicles provided by the dataset, instead of the whole fleet of the city. However, due to the advantage of random sampling and high coverage of road network, the results from the ride-hailing dataset can adequately reflect the relative traffic conditions and spatial distribution of BWP emissions but still need further verification with a full-sample test (Liu et al., 2019b).

According to the trip-level analysis in Section 4.2, these variations come from diverse driving speed and braking parameters. As shown in Fig. 7 (d) to (g), roads with the highest EFs (usually urban streets) are typically characterized by low driving speed and high braking frequency. For example, vehicles at intersections usually travel at a low speed (19.81 km/h on average) with frequent and short braking events (36.19 times per kilometer, 1.71 s per time). Meanwhile, the distribution of high EF intersection hotspots is mostly concentrated on the local roads (such as residential roads, links, and living streets, see Figure S6-2 and S6-3) where frequent stop-and-go happens. On the contrary, the EFs are relatively low on motorways and trunks where vehicles run faster (33.29 km/h on average) and brake infrequently (10.43 times per kilometer), while the emissions per braking on motorways and trunks are 1.33 times higher than at intersections (1.70 mg/braking versus 0.73 mg/braking). Therefore, although the intensity of each braking on motorways and trunks is greater, the cumulative amount is lower with less braking. As explained by SHAP, the similar spatial distributions of braking frequency and EF also indicate a high correlation.

4.4. Temporal BWP emission variations

Fig. 8 (a) shows the aggregation results for each date. The average BWP EF on each day varies from 24.40 to 26.52 mg/km/veh, with an average of 25.62 mg/km/veh. During the week, the EF usually reaches its lowest on Wednesday or Thursday and climbs to its

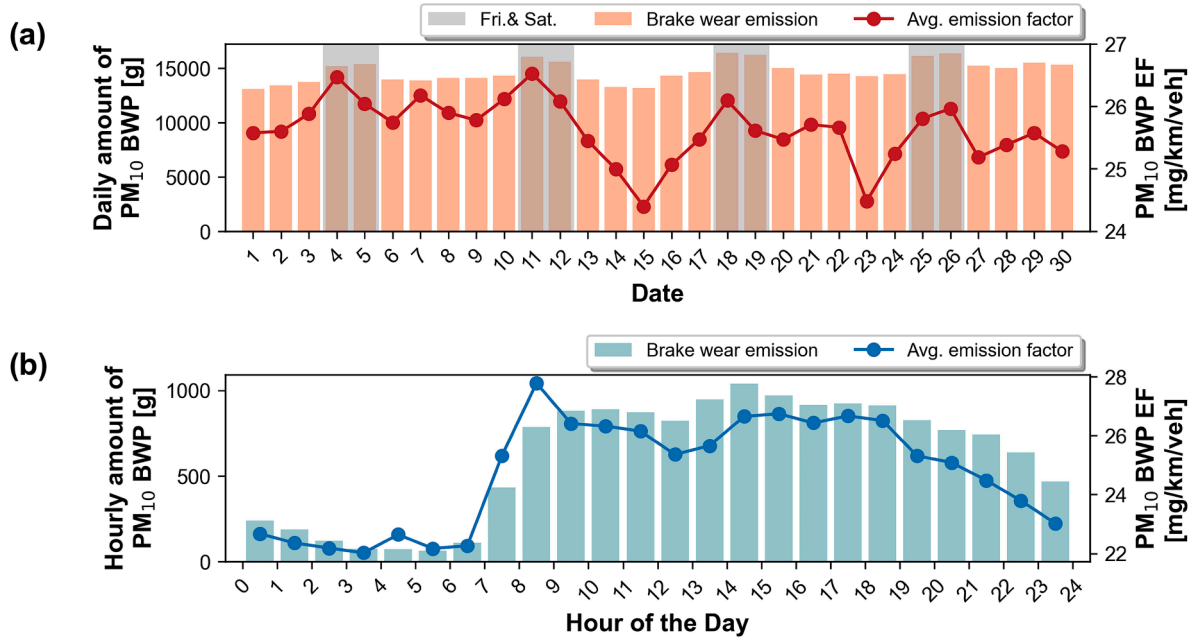

Fig. 8. PM_{10} BWP emissions amount and EF of (a) each date; and (b) each hour of the day from temporal aggregation.

highest on Friday or Saturday whose EFs are 2.41 % higher than the other days. Compared to the daily variations, hourly changes in BWP emissions are more significant. As shown in Fig. 8 (b), EFs between 0:00 and 7:00 are the lowest with an average of 22.33 mg/km/veh. During the morning peak (7:00 to 9:00), they increase dramatically and remain at a high level from 9:00 to 19:00 with an average of 26.33 mg/km/veh, followed by a slight decline after entering the night. The hourly PM_{10} BWP emissions share a similar variation with EFs.

The common feature of the daily and hourly variations is that EFs are higher during peak hours, Fridays, and Saturdays than in other non-rush periods. Meanwhile, the daily BWP emissions are also high in these periods, with more travel demand and ride-hailing requests (Figure S10-1). The explanation for these lies in the time-varying driving features (Figure S10-2). In rush periods, high traffic volume and congestion reduce the average speed of the fleet and lead to frequent braking for car-following, both of which would lead to high EFs, according to the previous analysis. Although harsh deceleration is more likely to occur during non-rush periods, their contributions are eliminated by low braking frequency.

5. Discussions

5.1. *The future of BWP emission modeling*

In this study, the OpMode-based model establishes a link between braking behavior and BWP emissions. Compared with the existing MOVES4 model, the proposed model improves ER estimation by considering braking deceleration distributions within each OpMode with the updated ER-deceleration curve (as discussed in S8). However, challenges in the BWP emission modeling still need to be addressed.

The first obstacle is the uncertainties of the ER-deceleration curve, which uses the drive-cycle-average braking deceleration to predict ERs. Results under the same cycle are affected by unregulated test specifications, introducing great variations that could be partially eliminated by adopting the new Global Technical Regulation of BWP emission measurements (Giechaskiel et al., 2024). However, information on braking provided by cycle-based measurement is still limited, emphasizing the need for parameterized measurements, which enables us to get rid of dependence on drive cycles for predicting BWP emissions from individual braking events to the macro emissions (Rahimi et al., 2023). In addition, our results suggest that future driving cycles designed for braking tests should include not only speed profiles but also braking frequency and intensity, which greatly impact the BWP with distinct regional and fleet-specific characteristics.

Another problem lies in the contradiction between the current OpMode definition and the deceleration-dependent ER prediction. The current OpMode definition follows the rule of exhaust emissions, while the application on BWP needs further classification. For example, braking records in the current "braking mode" cover the deceleration range from approximately 1 m/s^2 to 4.5 m/s^2 and the speed range from 3 km/h to 130 km/h, while the ERs are represented by only one value. The high proportion of braking in coasting also reflects the inconsistency between the current definition of OpMode and braking detection. Brake-specific OpModes suitable for BWP emissions need to be re-defined. Besides, braking detection methods should also be developed to facilitate the calibration of the power-based coastdown curve for distinguishing braking and coasting.

5.2. Potential impacts on vulnerable groups and mitigation efforts

The spatial emission distribution and the local POIs are illustrated in Fig. 9. BWP emission hotspots cover densely populated land use, including residential, commercial, healthcare, and education areas, with significant correlations with healthcare and commercial sites. Residents, especially vulnerable groups such as patients and children in these areas, will still face severe PM risk from BWP emissions, even when exhaust emissions are eliminated. This finding has rarely been revealed in previous studies, while this study uncovers the network-wide BWP hotspots for the first time, which largely extends the traffic-related air pollutant studies on the city scale. Given existing policies targeting exhaust emissions to reduce residents' exposure to pollutants, special attention should be paid to the mitigation of BWP emissions, according to the findings of this study.

Previous analyses suggest that braking frequency and traffic volume may be the predominant factors affecting BWP emissions in urban areas. High braking frequency is usually not an individual behavior but a fleet-wide driving pattern determined by road conditions (Zhou et al., 2024). For instance, vehicles on congested urban roads and intersections brake more frequently than on motorways. Therefore, reducing braking frequency is the key to the mitigation of BWP emissions. Although electric vehicles are claimed to reduce braking events by more than 50 % through regenerative braking, their emission reduction effect, which is affected by their excessive vehicle weight and unique emission characteristics, needs to be further quantified and verified (Beddows and Harrison, 2021; Liu et al., 2024; Mehlig et al., 2023; Zhang et al., 2024b). Beyond electric vehicles, other feasible measures to reduce stop-and-go operations should be adopted, especially in signalized intersections, including advanced traffic control methods (through signal coordination and adaptive timing) (Han et al., 2016), driving behavior guidance (through ecological driving and variable traffic information) (Li et al., 2024), and vehicle coordination (through vehicle platooning and autonomous driving) (Tu et al., 2019). Urban policy measures such as low-emission zones and better road designs to restrict the use of high-emitters and high-emitting operations can also be compared for the best practices to reduce road BWP. In that sense, the mitigation of BWP emissions shares similarities with exhaust emissions, while the optimization objective is different due to the nature of the emission generation process. The effect on BWP emissions can be more observable since exhaust emissions are also affected by factors such as fuel type, ambient temperature, and cold start operation (Jiang et al., 2024; Tu et al., 2022). These can be evaluated by combining traffic and multi-source emission simulations in the future (Naqvi et al., 2023).

This study recommends an average PM_{10} BWP EF of 27 $\pm$ 4 mg/km/veh for ride-hailing vehicles in the urban area, which is 3 to 4 times higher than the upcoming EURO 7 limit of 7 mg/km/veh (Ntziachristos et al., 2022). While regional differences and model uncertainties contribute to this high EF, it underscores the potential underestimation by current models and the challenge of meeting ambitious emission targets. Laboratory-tested solutions must be validated in real-world conditions and local assessments on large vehicle fleets to quantify their actual impact. In addition to BWP EF, more efforts should focus on quantifying its metallic composition in the airborne concentration from the BWP due to its severe health impacts. Dispersion simulations, exposure estimations, and real-world measurement verification should be tested in the future to construct a model chain for the impact assessment of non-exhaust emissions.

6. Conclusions

This study presents a comprehensive analysis of the brake wear particle (BWP) emissions from light-duty vehicles in urban areas, with a specific focus on ride-hailing vehicles. An operating-mode-based modeling framework was developed based on measurement results in the last two decades. Utilizing a substantial ride-hailing vehicle trajectory dataset from Chengdu, China, the model was applied with local survey data to estimate network-wide BWP emissions.

Our results reveal an average PM_{10} emission factor of 27 $\pm$ 4 mg/km/veh for ride-hailing vehicles in the study area, which is notably higher than previous findings due to frequent braking in the central city. A strong correlation was identified between the trip-level BWP emissions and driving parameters. This also unveils the potential for BWP emission reduction through improved driving behaviors and traffic management. The spatiotemporal analysis reveals that BWP emissions are concentrated in congested road sections and peak hours, which are typically characterized by high traffic volume and frequent braking. Meanwhile, the network-wide BWP hotspots were uncovered for the first time, linking emissions to areas for vulnerable groups like healthcare facilities. Our finding largely extends the traffic-related air pollutant studies on the city scale.

Our study reflects the urban environmental impact of ride-hailing vehicles after the removal of exhaust emissions in the future. Further verification using diverse data sources, including roadside measurement, mobile sampling, up-to-date driving trajectory, and local-context-based tests with different types of brake pads distinguished by factors such as components, brands, and use ages, is required to improve the representativeness and accuracy of the proposed BWP estimation model. Investigation regarding vehicle and brake specifications, including vehicle age distribution, brake pad materials, their lifespan, and braking control technology development should be conducted using varied data sources from manufacturers and vehicle management agencies. The potential for reducing BWP emissions in electric vehicles with greater mass and larger tire-road contact surfaces needs further exploration, especially in the context of rapid growth in traffic electrification. Furthermore, the modeling framework proposed in this study is expected to be extended to encompass wear emissions from tire-road contact, as they are influenced by common factors such as vehicle mass, kinematic parameters, and tire-road contact quality.

7. Code availability

Code for car sales data and market share data extraction are available at https://github.com/QiuziChen/car-sales-crawling.git and

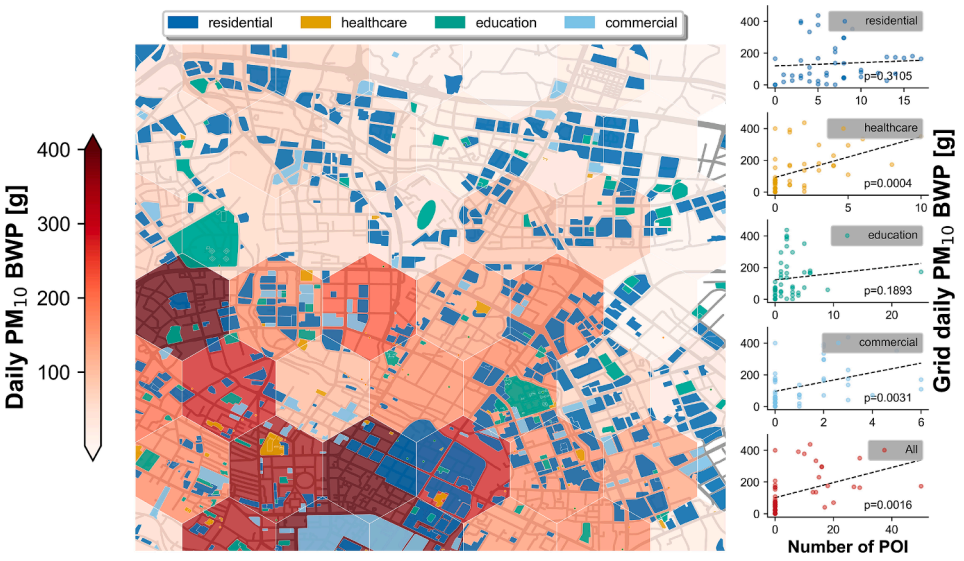

Fig. 9. Spatial distribution of points of interest in the study area with BWP emission hotspot. Four types of densely populated land use are plotted, including residential, healthcare, education, and commercial. The heatmap indicates the daily BWP emissions from ride-hailing vehicles of each hexagonal grid. The scatter diagrams show the linear correlation between grid daily PM_{10} BWP emissions with the number of corresponding land use types, p-value < 0.05 indicating a significant correlation.

https://github.com/QiuziChen/jd-comments-crawling.git, respectively. Code for trajectory data processing and BWP emission modeling are available at https://github.com/QiuziChen/brake-wear-emission-modeling.git.

CRediT authorship contribution statement

Qiuzi Chen: Writing – original draft, Visualization, Software, Methodology, Data curation, Conceptualization. **An Wang:** Writing – review & editing, Supervision. **Shunyao Wang:** Writing – review & editing, Funding acquisition. **Haobing Liu:** Writing – review & editing, Supervision, Funding acquisition. **Luyang Gong:** Resources, Funding acquisition. **Ran Tu:** Writing – review & editing, Supervision, Methodology, Investigation, Funding acquisition, Conceptualization.

Declaration of Competing Interest

The authors declare that they have no known competing financial interests or personal relationships that could have appeared to influence the work reported in this paper.

Acknowledgements

This study is supported by the National Key R&D Program of China (No. 2021YFE0112700), the National Natural Science Foundation of China (No. 52102409 & 22206119), the Natural Science Foundation of Jiangsu Province (No. BK20210246), the Fundamental Research Funds for the Central Universities (No. 242023R4002, 2023-4-YB-03), the Open Foundation of Key Laboratory of Transport Industry of Comprehensive Transportation Theory (Nanjing Modern Multimodal Transportation Laboratory) (No. MTF2023006), and the PuJiang Program from Science and Technology Commission of Shanghai Municipality (No. 22PJ1404100).

Appendix A. Supplementary data

Supplementary data to this article can be found online at https://doi.org/10.1016/j.trd.2024.104541.

Data availability

The data that support the findings of this study are available on request from the corresponding author upon reasonable request.

References

Alaska Satellite Facility, 2015. ALOS PALSAR Radiometric Terrain Correction (RTC) products. doi: 10.5067/Z97HFCNKR6VA.

Beddows, D.C.S., Harrison, R.M., 2021. PM10 and PM2.5 emission factors for non-exhaust particles from road vehicles: Dependence upon vehicle mass and implications for battery electric vehicles. Atmos. Environ. 244, 117886. https://doi.org/10.1016/j.atmosenv.2020.117886.

Bukowiecki, N., Lienemann, P., Hill, M., Furger, M., Richard, A., Amato, F., Prévôt, A.S.H., Baltensperger, U., Buchmann, B., Gehrig, R., 2010. PM10 emission factors for non-exhaust particles generated by road traffic in an urban street canyon and along a freeway in Switzerland. Atmos. Environ. 44, 2330–2340. https://doi.org/10.1016/j.atmosenv.2010.03.039.

Chang, S.Y., Huang, J., Chaveste, M.R., Lurmann, F.W., Eisinger, D.S., Mukherjee, A.D., Erdakos, G.B., Alexander, M., Knipping, E., 2023. Electric vehicle fleet penetration helps address inequalities in air quality and improves environmental justice. Commun Earth Environ 4, 135. https://doi.org/10.1038/s43247-023-00799-1.

Chen, T., Guestrin, C., 2016. XGBoost: A Scalable Tree Boosting System. doi: 10.48550/arXiv.1603.02754.

Chen, Q., Tu, R., 2024. Brake Wear Particle Emission Factors from Dynamometer Tests. https://doi.org/10.17632/crxjtgk5bg.1.

China Automotive Technology and Research Center, 2022. Terms and definitions of motor vehicles , trailers and combination vehicle-Part 1: Types.

Du, J., Ouyang, D., 2017. Progress of Chinese electric vehicles industrialization in 2015: A review. Appl. Energy 188, 529–546. https://doi.org/10.1016/j.apenergy.2016.11.129.

Gallus, J., Kirchner, U., Vogt, R., Benter, T., 2017. Impact of driving style and road grade on gaseous exhaust emissions of passenger vehicles measured by a Portable Emission Measurement System (PEMS). Transp. Res. Part D: Transp. Environ. 52, 215–226. https://doi.org/10.1016/j.trd.2017.03.011.

Garg, B.D., Cadle, S.H., Mulawa, P.A., Groblicki, P.J., Laroo, C., Parr, G.A., 2000. Brake Wear Particulate Matter Emissions. Environ. Sci. Technol. 34, 4463–4469. https://doi.org/10.1021/es001108h.

Giechaskiel, B., Grigoratos, T., Dilara, P., Karageorgiou, T., Ntziachristos, L., Samaras, Z., 2024. Light-Duty Vehicle Brake Emission Factors. Atmos. 15, 97. https://doi.org/10.3390/atmos15010097.

Grange, S.K., Fischer, A., Zellweger, C., Alastuey, A., Querol, X., Jaffrezo, J.-L., Weber, S., Uzu, G., Hueglin, C., 2021. Switzerland's PM10 and PM2.5 environmental increments show the importance of non-exhaust emissions. Atmos. Environ. X 12, 100145. https://doi.org/10.1016/j.aeaoa.2021.100145.

Grigoratos, T., Martini, G., 2015. Brake wear particle emissions: a review. Environ Sci Pollut Res 22, 2491–2504. https://doi.org/10.1007/s11356-014-3696-8.

Grigoratos, T., Mathissen, M., Vedula, R., Mamakos, A., Agudelo, C., Gramstat, S., Giechaskiel, B., 2023. Interlaboratory Study on Brake Particle Emissions—Part I: Particulate Matter Mass Emissions. Atmos. 14, 498. https://doi.org/10.3390/atmos14030498.

Hagino, H., Oyama, M., Sasaki, S., 2016. Laboratory testing of airborne brake wear particle emissions using a dynamometer system under urban city driving cycles. Atmos. Environ. 131, 269–278. https://doi.org/10.1016/j.atmosenv.2016.02.014.

Han, K., Liu, H., Gayah, V.V., Friesz, T.L., Yao, T., 2016. A robust optimization approach for dynamic traffic signal control with emission considerations. Transp. Res. Part C Emerging Technol. 70, 3–26. https://doi.org/10.1016/j.trc.2015.04.001.

Harrison, R.M., Jones, A.M., Gietl, J., Yin, J., Green, D.C., 2012. Estimation of the Contributions of Brake Dust, Tire Wear, and Resuspension to Nonexhaust Traffic Particles Derived from Atmospheric Measurements. Environ. Sci. Technol. 46, 6523–6529. https://doi.org/10.1021/es300894r.

Iijima, A., Sato, K., Yano, K., Kato, M., Kozawa, K., Furuta, N., 2008. Emission Factor for Antimony in Brake Abrasion Dusts as One of the Major Atmospheric Antimony Sources. Environ. Sci. Technol. 42, 2937–2942. https://doi.org/10.1021/es702137g.

Jeong, C.-H., Wang, J.M., Hilker, N., Debosz, J., Sofowote, U., Su, Y., Noble, M., Healy, R.M., Munoz, T., Dabek-Zlotorzynska, E., Celo, V., White, L., Audette, C., Herod, D., Evans, G.J., 2019. Temporal and spatial variability of traffic-related PM2.5 sources: Comparison of exhaust and non-exhaust emissions. Atmos. Environ. 198, 55–69. https://doi.org/10.1016/j.atmosenv.2018.10.038.

Jiang, Y., Song, G., Wu, Y., Lu, H., Zhai, Z., Yu, L., 2024. Impacts of cold starts and hybrid electric vehicles on on-road vehicle emissions. Transp. Res. Part D: Transp. Environ. 126, 104011. https://doi.org/10.1016/j.trd.2023.104011.

Kim, S.-H., Shim, W., Kwon, S.-U., Lee, J.-J., Seo, M.-W., Kim, J.-K., Pee, J.-H., Kim, J.-Y., 2020. The Impact of Composition in Non-steel and Low-Steel Type Friction Materials on Airborne Brake Wear Particulate Emission. Tribol Lett 68, 118. https://doi.org/10.1007/s11249-020-01361-2.

Lee, E.S., Sahay, K., O'Neil, E., Biswas, S., Dzhema, I., Huang, S.-M., Lin, P., Chang, M.-C.-O., Huai, T., 2023. Tracer-Gas-Integrated Measurements of Brake-Wear Particulate Matter Emissions from Heavy-Duty Vehicles. Environ. Sci. Technol. 57, 15968–15978. https://doi.org/10.1021/acs.est.3c03673.

Li, W., Ding, H., Xu, N., Zhang, J., 2024. Toward Carbon-Neutral Transportation Electrification: A Comprehensive and Systematic Review of Eco-Driving for Electric Vehicles. IEEE Trans. Transp. Electrific. 10, 6340–6360. https://doi.org/10.1109/TTE.2023.3331727.

Liu, Y., Wu, S., Chen, H., Federici, M., Perricone, G., Li, Y., Lv, G., Munir, S., Luo, Z., Mao, B., 2022. Brake wear induced PM10 emissions during the world harmonised light-duty vehicle test procedure-brake cycle. J. Clean. Prod. 361, 132278. https://doi.org/10.1016/j.jclepro.2022.132278.

Liu, Y., Chen, H., Jiang, L., Li, T., Guo, J., Wei, T., Crowther, R., 2024. Environmental and health impacts of banning passenger cars with internal combustion engines: A case study of Leeds, UK. Transp. Res. Part D: Transp. Environ. 134, 104343. https://doi.org/10.1016/j.trd.2024.104343.

Liu, J., Han, K., Chen, X., (Michael), Ong, G.P., 2019b. Spatial-temporal inference of urban traffic emissions based on taxi trajectories and multi-source urban data. Transp. Res. Part C Emerging Technol. 106, 145–165. https://doi.org/10.1016/j.trc.2019.07.005.

Liu, H., Rodgers, M.O., Guensler, R., 2019a. The impact of road grade on vehicle accelerations behavior, PM2.5 emissions, and dispersion modeling. Transp. Res. Part D: Transp. Environ. 75, 297–319. https://doi.org/10.1016/j.trd.2019.09.006.

Lundberg, S.M., Erion, G., Chen, H., DeGrave, A., Prutkin, J.M., Nair, B., Katz, R., Himmelfarb, J., Bansal, N., Lee, S.-I., 2020. From local explanations to global understanding with explainable AI for trees. Nat Mach Intell 2, 56–67. https://doi.org/10.1038/s42256-019-0138-9.

Matthaios, V.N., Lawrence, J., Martins, M.A.G., Ferguson, S.T., Wolfson, J.M., Harrison, R.M., Koutrakis, P., 2022. Quantifying factors affecting contributions of roadway exhaust and non-exhaust emissions to ambient PM10–2.5 and PM2.5–0.2 particles. Sci. Total Environ. 835, 155368. https://doi.org/10.1016/j.scitotenv.2022.155368.

Mehlig, D., Staffell, I., Stettler, M., ApSimon, H., 2023. Accelerating electric vehicle uptake favours greenhouse gas over air pollutant emissions. Transp. Res. Part D: Transp. Environ. 124, 103954. https://doi.org/10.1016/j.trd.2023.103954.

Naqvi, A., Peer, S., Müller, J., Straub, M., 2023. The spatial–temporal exposure to traffic-related Particulate Matter emissions. Transp. Res. Part D: Transp. Environ. 123, 103899. https://doi.org/10.1016/j.trd.2023.103899.

L. Ntziachristos P. Boulter EMEP/EEA air pollutant emission inventory guidebook 2023 2023 – Update 2023.

Ntziachristos, L., Papadopoulos, G., Samos, Z., Tsalikidis, N., Mellios, G., Dimaratos, A., Kontses, A., Kontses, D., Samaras, Z., 2022. European Commission, Directorate-General for Internal Market. Industry, Entrepreneurship and SMEs, Euro 7 Impact Assessment Study. Publications Office of the European Union.

Oroumiyeh, F., Zhu, Y., 2021. Brake and tire particles measured from on-road vehicles: Effects of vehicle mass and braking intensity. Atmos. Environ.: X 12, 100121. https://doi.org/10.1016/j.aeaoa.2021.100121.

Piscitello, A., Bianco, C., Casasso, A., Sethi, R., 2021. Non-exhaust traffic emissions: Sources, characterization, and mitigation measures. Sci. Total Environ. 766, 144440. https://doi.org/10.1016/j.scitotenv.2020.144440.

Rahimi, M., Candeo, S., Da Lio, M., Biral, F., Wahlström, J., Bortoluzzi, D., 2023. A novel approach for brake emission estimation based on traffic microsimulation, vehicle system dynamics, and machine learning modeling. Atmos. Pollut. Res. 14, 101872. https://doi.org/10.1016/j.apr.2023.101872.

Ren, J., Yeoh, W., Shan Ee, M., Popovič, A., 2018. Online consumer reviews and sales: Examining the chicken-egg relationships. Asso for Info Science & Tech 69, 449–460. https://doi.org/10.1002/asi.23967.

Sanders, P.G., Xu, N., Dalka, T.M., Maricq, M.M., 2003. Airborne Brake Wear Debris: Size Distributions, Composition, and a Comparison of Dynamometer and Vehicle Tests. Environ. Sci. Technol. 37, 4060–4069.

Sarica, T., Chaillou, C., Roustan, Y., Larrieu, C., Wali, S.-E., Sartelet, K., 2024. Differentiated impact of low-exhaust-emission vehicles on NO2 and particle concentrations in the Paris region. Eur. Transp. Res. Rev. 16, 34. https://doi.org/10.1186/s12544-024-00660-2.

Singh, V., Biswal, A., Kesarkar, A.P., Mor, S., Ravindra, K., 2020. High resolution vehicular PM10 emissions over megacity Delhi: Relative contributions of exhaust and non-exhaust sources. Sci. Total Environ. 699, 134273. https://doi.org/10.1016/j.scitotenv.2019.134273.

Storch, L., Hamatschek, C., Hesse, D., Feist, F., Bachmann, T., Eichler, P., Grigoratos, T., 2023. Comprehensive Analysis of Current Primary Measures to Mitigate Brake Wear Particle Emissions from Light-Duty Vehicles. Atmos. 14, 712. https://doi.org/10.3390/atmos14040712.

Sun, D., Zhang, K., Shen, S., 2018. Analyzing spatiotemporal traffic line source emissions based on massive didi online car-hailing service data. Transp. Res. Part D: Transp. Environ. 62, 699–714. https://doi.org/10.1016/j.trd.2018.04.024.

The California Air Resources Board, 2021. EMFAC2021 Technical Document.

Tomar, G., Nagpure, A.S., Kumar, V., Jain, Y., 2022. High resolution vehicular exhaust and non-exhaust emission analysis of urban-rural district of India. Sci. Total Environ. 805, 150255. https://doi.org/10.1016/j.scitotenv.2021.150255.

Tortora, M., Cordelli, E., Soda, P., 2022. PyTrack: A Map-Matching-Based Python Toolbox for Vehicle Trajectory Reconstruction. IEEE Access 10, 112713–112720. https://doi.org/10.1109/ACCESS.2022.3216565.

Tu, R., Alfaseeh, L., Djavadian, S., Farooq, B., Hatzopoulou, M., 2019. Quantifying the impacts of dynamic control in connected and automated vehicles on greenhouse gas emissions and urban NO2 concentrations. Transp. Res. Part D: Transp. Environ. 73, 142–151. https://doi.org/10.1016/j.trd.2019.06.008.

Tu, R., Xu, J., Wang, A., Zhang, M., Zhai, Z., Hatzopoulou, M., 2022. Real-world emissions and fuel consumption of gasoline and hybrid light duty vehicles under local and regulatory drive cycles. Sci. Total Environ. 805, 150407. https://doi.org/10.1016/j.scitotenv.2021.150407.

USEPA, 2020. Brake and Tire Wear Emissions from Onroad Vehicles in MOVES3 No. EPA-420-R-20-014, USEPA.

Wei, N., Jia, Z., Men, Z., Ren, C., Zhang, Y., Peng, J., Wu, L., Wang, T., Zhang, Q., Mao, H., 2022. Machine Learning Predicts Emissions of Brake Wear $PM_{2.5}$: Model Construction and Interpretation. Environ. Sci. Technol. Lett. 9, 352–358. https://doi.org/10.1021/acs.estlett.2c00117.

Woo, S.-H., Kim, Y., Lee, S., Choi, Y., Lee, S., 2021. Characteristics of brake wear particle (BWP) emissions under various test driving cycles. Wear 480–481, 203936. https://doi.org/10.1016/j.wear.2021.203936.

Wu, J., Jia, P., Feng, T., Li, H., Kuang, H., 2023. Spatiotemporal analysis of built environment restrained traffic carbon emissions and policy implications. Transp. Res. Part D: Transp. Environ. 121, 103839. https://doi.org/10.1016/j.trd.2023.103839.

Zhai, Z., Song, G., Liu, Y., Cheng, Y., He, W., Yu, L., 2019. Characteristics of operating mode distributions of light duty vehicles by road type, average speed, and driver type for estimating on-road emissions: Case study of Beijing. J. Intell. Transp. Syst. 23, 191–202. https://doi.org/10.1080/15472450.2018.1528447.

Zhang, Q., Fang, T., Men, Z., Wei, N., Peng, J., Du, T., Zhang, X., Ma, Y., Wu, L., Mao, H., 2024a. Direct measurement of brake and tire wear particles based on real-world driving conditions. Sci. Total Environ. 906, 167764. https://doi.org/10.1016/j.scitotenv.2023.167764.

Zhang, J., Peng, J., Song, C., Ma, C., Men, Z., Wu, J., Wu, L., Wang, T., Zhang, X., Tao, S., Gao, S., Hopke, P.K., Mao, H., 2020. Vehicular non-exhaust particulate emissions in Chinese megacities: Source profiles, real-world emission factors, and inventories. Environ. Pollut. 266, 115268. https://doi.org/10.1016/j.envpol.2020.115268.

Zhang, Q., Yin, J., Fang, T., Guo, Q., Sun, J., Peng, J., Zhong, C., Wu, L., Mao, H., 2024b. Regenerative braking system effectively reduces the formation of brake wear particles. J. Hazard. Mater. 465, 133350. https://doi.org/10.1016/j.jhazmat.2023.133350.

Zhou, Y., Fu, C., Jiang, X., Yu, Q., Liu, H., 2024. Who might encounter hard-braking while speeding? Analysis for regular speeders using low-frequency taxi trajectories on arterial roads and explainable AI. Accid. Anal. Prev. 195, 107382. https://doi.org/10.1016/j.aap.2023.107382.